THE JOURNAL OF PHYSICAL CHEMISTRY Letters

Letter

pubs.acs.org/JPCL

Analysis of the Hysteresis Behavior of Perovskite Solar Cells with Interfacial Fullerene Self-Assembled Monolayers

Marta Valles-Pelarda,[†] Bruno Clasen Hames,[†] Inés García-Benito,[‡,§] Osbel Almora,[†] Agustin Molina-Ontoria,[‡] Rafael S. Sánchez,[†] Germa Garcia-Belmonte,[†] Nazario Martín,*[,‡,§] and Ivan Mora-Sero*[,†]

[†]Institute of Advanced Materials (INAM), Universitat Jaume I, Avenida Sos Baynat, s/n, 12006 Castellón, Spain

[‡]IMDEA-Nanociencia, C/Faraday 9, Campus de la Universidad Autónoma de Madrid, E-28049 Madrid, Spain

[§]Departamento de Química Orgánica. Facultad de Ciencias Químicas, Universidad Complutense de Madrid, E-28040 Madrid, Spain

Supporting Information

ABSTRACT: The use of self-assembled monolayers (SAMs) of fullerene derivatives reduces the hysteresis of perovskite solar cells (PSCs). We have investigated three different fullerene derivatives observing a decrease on hysteresis for all the cases. Several processes can contribute to the hysteresis behavior on PSCs. We have determined that the reduced hysteresis observed for devices with SAMs is produced by a decrease of the capacitive hysteresis. In addition, with an appropriated functionalization, SAMs can increase photocurrent even when no electron selective contact (ESC) is present and a SAM is deposited just on top of the transparent conductive oxide. Appropriated functionalization of the fullerene derivative, as introducing −CN groups, can enhance cell performance and reduce hysteresis. This work paves the way for a future enhancement of PSCs by a tailored design of the fullerene molecules that could actuate as an ESC by themselves.

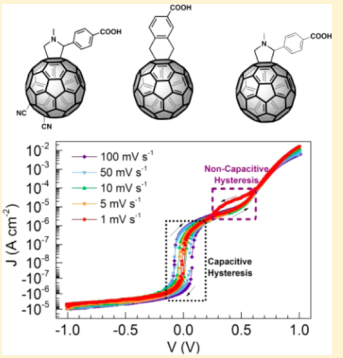

After the first reports on all-solid perovskite solar cells (PSCs),[1,2] the interest of the scientific community on this kind of devices has boosted. Successive improvements of the cell configuration, deposition methods, perovskite composition (combination of organic and inorganic cations with halide anions), as well as hole and electron transporting materials[3−7] have produced record certified devices with efficiencies as high as 22.1%.[8] Nevertheless, despite the spectacular enhancement in very few years, many aspects related to the behavior of halide perovskites and to the working principles of PSCs remain unclear and are still under debate. One of these debates is the role of the charge selective contacts, not only in terms of the overall efficiency but also in terms of the anomalous phenomena widely observed in PSCs; for instance, the hysteresis present in the Current−Potential (J−V) curves. Many different contacts have been studied for PSCs, which show their important role on the solar cell efficiency, stability, and hysteresis.[9,10]It is commonly established that the use of fullerene derivatives in PSCs with inverted configuration produces devices without J−V hysteresis; however, recent papers demonstrate that this statement cannot be generalized, for example, significant hysteresis has been detected at low temperature even with the presence of fullerene derivatives.[11,12] Hysteresis in inverted configuration devices appears in different conditions and shows different and using TiO_2 mesoporous scaffold.[11,13,14] In this communication, we have studied the effect of a self-assembled monolayer (SAM) of different fullerene derivatives specifically functionalized to anchor to an oxide surface. The effect of the anchoring moiety, the insertion of additional functional groups in the fullerene unit for a more intimate contact with the perovskite, and the role of compact selective contacts have been analyzed by focusing on the solar cell performance and hysteresis.

Very recently, capacitive and noncapacitive components, whose origins are believed to arise from different physical and/or chemical mechanisms, have been identified in the hysteresis of PSCs.[14] Capacitive hysteresis is directly proportional to the current−potential (J−V) curve scan rate, s. A capacitor with capacitance C presents a measured current $s{\cdot}C$ in the J−V curve observed during the voltage sweep. The change of the scan rate direction consequently produces a change in the sign of the current provoking the hysteresis. Moreover noncapacitive hysteresis is not proportional to scan rate and has a different physical origin, as we discuss below. We have observed that perovskite solar cells (PSCs) prepared with a SAM of fullerene derivatives present a mixed hysteresis behavior: first, they exhibit the typical capacitive component of a standard PSCs prepared with TiO_2 as an electron selective contact (ESC), although the hysteresis is significantly less pronounced when the fullerene SAM is introduced; second, a noncapacitive hysteresis previously observed also in inverted PSCs with fullerene was also detected in PSCs with a SAM.

Received: September 14, 2016
Accepted: October 31, 2016
Published: October 31, 2016

DOI: 10.1021/acs.jpclett.6b02103
J. Phys. Chem. Lett. XXXX, XXX, XXX−XXX

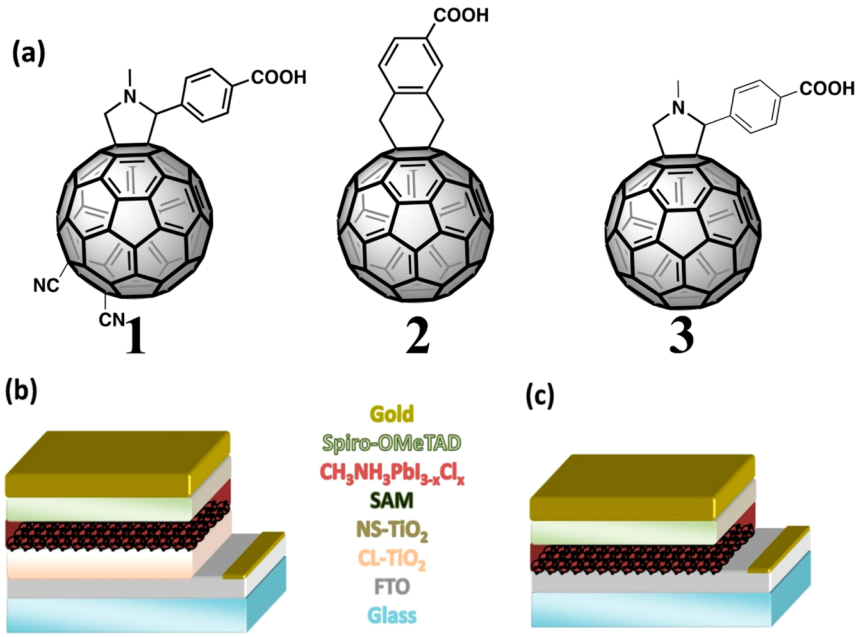

Figure 1. (a) Functionalized fullerenes studied in this work. Configuration of the perovskite solar cell analyzed in this work; devices (b) with (CL) and (c) without (NCL) TiO_2 compact layer on top of FTO have been analyzed. Nanostructured TiO_2 layer ($NS\text{-}TiO_2$) was used for all the samples.

The photovoltaic performance does not only depend on the light absorbing material but also on the efficient charge extraction at the selective contacts.[15] TiO_2 is probably the most extensively used ESC in PSCs, although organic ESCs are receiving increasing attention.[16] In accordance with this, it has been shown that the use of fullerene derivative layers,[17,18] the deposition of a thin fullerene layer,[19,20] or even the use of a SAM on top of a TiO_2,[21] significantly reduces the photoluminescence lifetime, thus indicating a better electron extraction when the fullerene derivatives substitute the TiO_2 or even when the fullerene is on the top of the TiO_2 layer. Therefore, modifying the ESC-perovskite interface can significantly enhancethe electron injection and electron transfer, as well as reducing the charge recombination.[19,21] As it has previously been stated, the approach that consists in functionalizing the ESC with fullerene derivatives has been investigated in this work. Fullerenes have high electron affinity and are good electron acceptors. Their π-conjugated structure enables the charge delocalization, thus enhancing the electron extraction. As it has already been mentioned, fullerenes have reduced the hysteresis effect observed in PSCs from the standard $J-V$ measurements. In this sense, it is especially interesting to analyze how a single fullerene monolayer can affect the ESC-perovskite interface properties. It is worth pointing out that such interesting approach constitutes a valuable tool for a better understanding of the hysteresis origins and its subsequent minimization, while it is based on easy and material-saving procedures compared to the approach based on the exploitation of a thin layer of a fullerene derivative. Additionally, we have also analyzed how the SAM of the fullerene derivatives behave when no compact TiO_2 layer is employed; in particular, we have observed that the deleterious effect of removing the compact TiO_2 can be relatively mitigated by the presence of the SAM. The presence of compact TiO_2 and/or fullerene derivative SAM has a huge impact on the $J-V$ hysteresis, and an appropriate choice of the fullerene derivative can avoid the photocurrent reduction observed when no compact TiO_2 is used.

In this work, we have analyzed three different fullerene derivatives (**1**−**3**; see Figure 1a), whose syntheses is described in detail in the Methods section. The fullerene derivatives have been functionalized with a carboxyl group (−COOH), which is a widely employed functional group for anchoring to the TiO_2 surface. We have selected as a reference the fullerene derivative **3**, already reported in the literature,[21] where a benzoic acid is linked to the fullerene through a *N*-methylpyrrolidine, and we have prepared a couple of variations by changing, on one hand, the connection between the fullerene and the benzoic acid (using a cyclohexane instead of a pyrrolidine). On the other hand, we have introduced two cyanide groups in the fullerene moiety, which significantly modify the reduction potential values of the molecule and provide further anchoring group through the lone pair nitrogen atoms, see Figure 1a. These modifications have allowed us to study not only the influence of the bridging functional group that connects the fullerene with the oxide substrate, but also the influence of the functional groups that contact directly with the perovskite layer, i.e., the cyanide groups from **1** (see Figure 1a). The optical absorption of the fullerene derivatives has been analyzed (see Figure S1; very similar features have been observed, and a band gap of ∼2 eV has been estimated for all three fullerene derivatives (see Table S1). In addition, the HOMO and LUMO energies and the redox potentials (see Table S2) have been measured using cyclic voltammetry (see Figure S2).

In order to analyze the effect of the fullerene derivatives, we have selected the probably most extended configuration for PSCs (see Figure 1b). In this configuration, a compact layer (CL) of TiO_2 is deposited on top of a glass/FTO substrate. A mesoporous layer of TiO_2 has been subsequently deposited. The deposited perovskite $CH_3NH_3PbI_3$, hereafter $MAPbI_3$, not only infiltrates into the mesoporous layer of TiO_2 but also produces a perovskite capping layer on top (see Figure S3). Finally, spiro-OMeTAD as a hole selective contact (HSC) and a gold layer are deposited in order to efficiently extract the photogenerated holes. A similar configuration but with no TiO_2 compact layer (NCL) has also been studied (see Figure 1c).

DOI: 10.1021/acs.jpclett.6b02103
J. Phys. Chem. Lett. XXXX, XXX, XXX−XXX

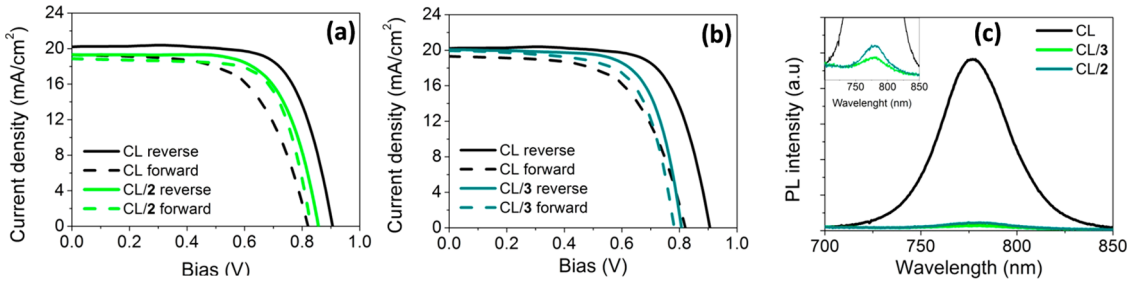

Figure 2. Current−voltage curves for forward and reverse scans for perovskite solar cell with a SAM of (a) **2** and (b) **3**. (c) Photoluminescence intensity of reference sample and samples with SAM of **2** and **3**.

Table 1. Characteristic Parameters of the Solar Cells Analyzed in This Work: Short Circuit Current, J_{sc}, Open Circuit Voltage, V_{oc}, Fill Factor, FF, and Photoconversion Efficiency, η[a]

device	scan direction	J_{sc} (mA/cm^2)	V_{oc} (mV)	FF (%)	η (%)	HI
CL	reverse	19.8 ± 0.6	909 ± 15	75.4 ± 2.1	13.5 ± 0.6	0.067 ± 0.004
	forward	19.3 ± 0.6	827 ± 18	63.4 ± 2.2	10.1 ± 0.7	
CL/3	reverse	19.2 ± 0.5	822 ± 13	71.4 ± 1.9	11.2 ± 0.3	0.019 ± 0.005
	forward	18.7 ± 0.8	797 ± 15	70.3 ± 2.0	10.47 ± 0.22	
CL/2	reverse	19.2 ± 0.6	839 ± 12	67 ± 4	10.9 ± 0.8	0.036 ± 0.003
	forward	18.7 ± 0.5	818 ± 8	66 ± 5	10.0 ± 0.8	
device	scan direction	J_{sc} (mA/cm^2)	V_{oc} (mV)	FF (%)	Eff (%)	
CL	reverse	17.1 ± 1.3	792 ± 18	68 ± 5	9.1 ± 0.9	0.20 ± 0.07
	forward	14.5 ± 2.2	728 ± 54	49 ± 9	5.4 ± 1.7	
NCL	reverse	11.9 ± 0.1.7	817 ± 16	64 ± 5	6.2 ± 1.0	0.32 ± 0.03
	forward	11.2 ± 1.8	768 ± 35	41 ± 3	3.6 ± 0.7	
CL/1	reverse	18.1 ± 1.3	780 ± 11	63 ± 13	8.9 ± 1.9	0.092 ± 0.016
	forward	16.6 ± 0.9	779 ± 6	71.4 ± 2.1	9.2 ± 0.5	
NCL/1	reverse	17.4 ± 1.9	753 ± 17	64 ± 6	8.4 ± 1.6	0.198 ± 0.014
	forward	14 ± 3	708 ± 61	43 ± 6	4.4 ± 1.3	

[a]Averaged values and the corresponding standard errors have been calculated using the results obtained by at least 10 cells prepared at each condition (see Table S3 and S4). Two different set of samples have been prepared with their corresponding reference samples, in order to compare samples produced with the same experimental conditions. Samples were prepare under air atmosphere and temperature and humidity conditions vary from batch to batch. Consequently, we compare samples containing SAM with reference samples produced in the same batch. The hysteresis index (HI) was calculated using eq 1 for the $J-V$ curves shown in Figures 2 and 3.

Reference samples have been produced by the direct deposition of perovskite on the bare substrates, while devices with interfacial fullerene derivative SAM have been produced by dipping the TiO_2 substrates in a chlorobenzene solution containing the desired fullerene derivative for 24 h (see the Methods section for more details. After the SAM deposition, the surface nature of the substrate is clearly modified, which is manifested through a greater hydrophobicity of the surface.

The effect of using **2** and **3** derivatives on the cell performance can be observed in the $J-V$ curves under 1 sun illumination, plotted in Figure 2a,b, respectively. The reference sample, using the configuration reported in Figure 1b with compact layer and without SAM, is denoted as the CL sample. Samples with **2** and **3** SAMs are called CL/**2** (Figure 2a) and CL/**3** (Figure 2b), respectively. The averaged values of the solar cell parameters are summarized in Table 1. It can be clearly observed that the most conspicuous effect of the presence of the SAM is a clear reduction of the hysteresis. The properties of the TiO_2-perovskite interfaces have been modified after SAM deposition, as can be clearly observed from the strong quenching of the photoluminescence (PL) (see Figure 2c), conventionally attributed to an improved charge extraction.[21] However, in contrast to previous reports,[21] we have not detected any increase of the photocurrent, which is not altered or is even slightly reduced when the fullerene SAM is introduced (see Figure 2a,b), respectively. In addition, the slight decrease of V_{oc} detected for samples with SAM and the larger dark current detected when SAM is used, in some cases (see Figure S4), makes that it is not possible to discard an increase of the recombination when SAM is used.

The observed hysteresis has been quantified by calculating the HI as follows:[22]

$$\mathrm{HI} = \frac{j_{rev}(V_{oc}/2) - j_{for}(V_{oc}/2)}{j_{rev}(V_{oc}/2)} \quad (1)$$

where $J_{rev}(V_{oc}/2)$ and $J_{for}(V_{oc}/2)$ are the currents when half of the V_{oc} voltage is applied for reverse (from V_{oc} to zero) and for forward (from zero to V_{oc}) voltage scans, respectively. A device without hysteresis presents a HI of zero, while higher values of HI indicate a more pronounced hysteresis. When **2** and **3** SAMs are used, the HI is significantly reduced, 2- and 4-fold, respectively.

In order to gain further insight about the particularities of the observed hysteresis for samples with fullerene derivatives, $J-V$ curves under dark with different scan rates have been measured (see Figure 3). The hysteresis observed in PSCs does not have a single and general origin for all the cases. Very recently, it has been shown that the $J-V$ hysteresis under dark of standard devices using TiO_2/spiro-OMeTAD as ESC/HSC has a

DOI: 10.1021/acs.jpclett.6b02103
J. Phys. Chem. Lett. XXXX, XXX, XXX−XXX

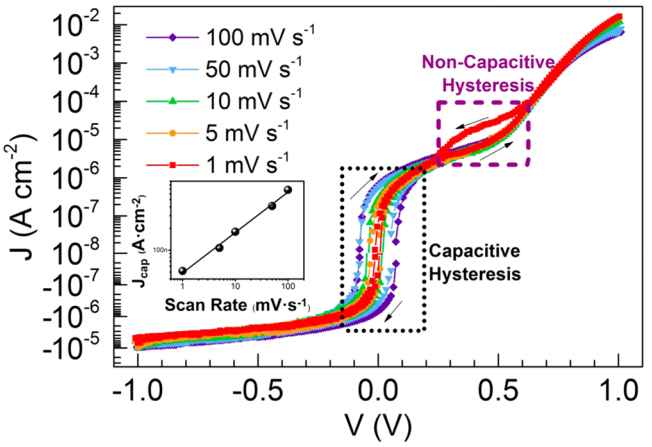

Figure 3. Dark $J-V$ curves in logarithm scaled current representation at different scan rates for a perovskite solar cell with a SAM of **3**. Capacitive hysteresis dependent on the scan rate is highlighted with a dotted frame, while noncapacitive hysteresis not observed at high scan rates is highlighted with a dashed frame. Black arrows indicate the scan direction. Inset: capacitive current, J_{cap}, versus scan rate, symbols represent the experimental points while solid line is the linear fit. J_{cap} is the contribution of the capacitive current.[14]

capacitive origin that is directly proportional to the scan rate.[14,23] This hysteresis is observed at low applied voltages, and we have also observed it when the fullerene derivative SAMs are deposited, see dotted frame in Figure 3, and its dependence with the scan rate in the inset of Figure 3. Additionally, we have also observed another hysteresis feature at applied voltages of around 0.5 V at very low scan rates, and consequently this is believed to arise from a noncapacitive process (see dashed frame in Figure 3). Inverted noncapacitive hysteresis under dark has been observed for inverted PSCs using PEDOT/PCBM as HSC/ESC; however, the noncapacitive hysteresis is still observed for standard PSCs with TiO_2 contact, but it is in general less evident. It has been suggested that the origin of noncapacitive hysteresis could be related to the reactivity of the perovskite at the interface with the contact.[14,24] This noncapacitive hysteresis has been also observed in devices in which neither TiO_2 nor organic electron conductors played a role as symmetrical Au/perovskite/Au samples and explained in that case by the formation of blocking contacts at the perovskite/Au interface and the modification of these contact properties following strong polarization.[25] A more systematic study will be needed to unveil the single or multiple origin of noncapacitive hysteresis in each case. While capacitive hysteresis just makes the determination of solar cell parameters difficult and will not have any effect at cell working DC conditions, the determination of the physical origin/s of nonradiative hysteresis could have important implications in PSCs. It will be especially important if the physical origin is related to surface reactivity, as it could limit the long-term solar cell stability.

Interestingly, the observed noncapacitive hysteresis behavior has an inverted nature, first observed by Almora et al.,[14] compared to the capacitive hysteresis (see black arrows in Figure 3). Moreover, very recently, inverted hysteresis under illumination has been also reported for mixed-halide mixed-

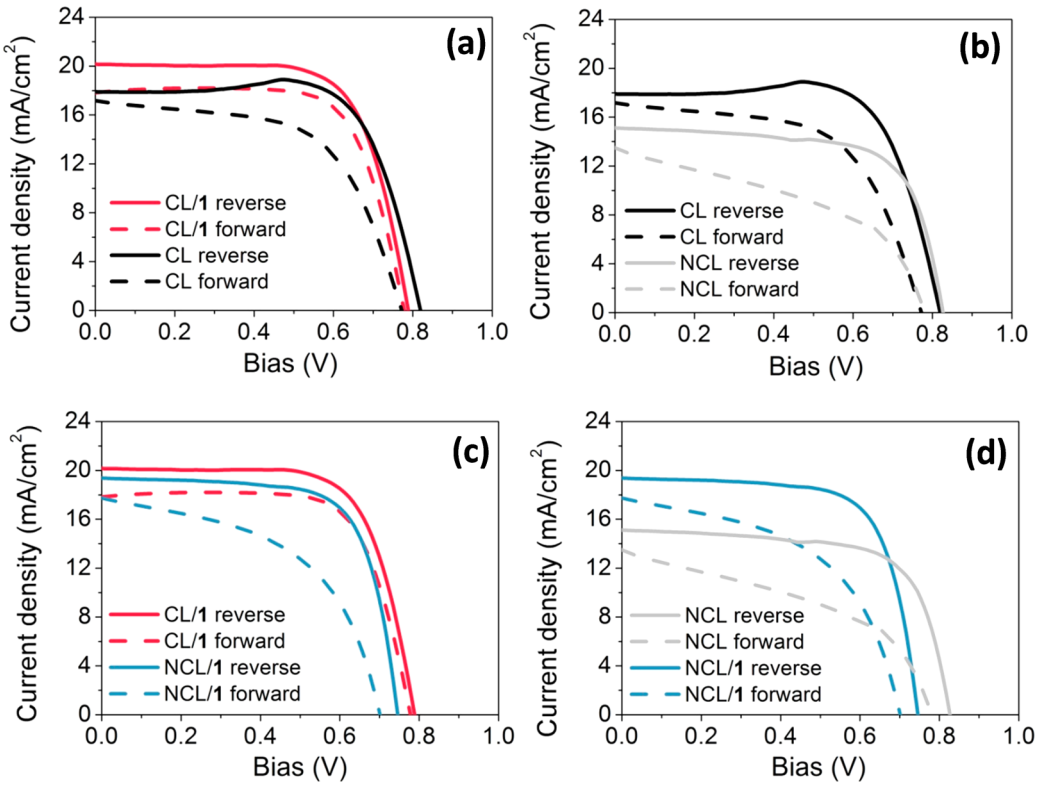

Figure 4. $J-V$ curves for forward and reverse scans under 1 sun illumination comparing samples with and without fullerene **1** SAM. (a) Perovskite solar cells with compact layer (CL) of TiO_2 with and without a SAM of **1**. (b) Perovskite solar cells without SAM comparing samples with compact layer (CL) of TiO_2 and with no compact layer (NCL) of TiO_2. (c) Perovskite solar cells with SAM of **1** comparing samples with compact layer (CL) of TiO_2 and with no compact layer (NCL) of TiO_2. (d) Perovskite solar cells with no compact layer (CL) of TiO_2 comparing samples with and without a SAM of **1**.

DOI: 10.1021/acs.jpclett.6b02103
J. Phys. Chem. Lett. XXXX, XXX, XXX−XXX

organic cation perovskites and in $MAPbI_3$ devices with a mesoporous TiO_2 scaffold covered with a thin insulating Al_2O_3 shell, and its origin is attributed to an energetic extraction barrier at the TiO_2 interface with dipole layer formation.[26] In both cases, a clear interfacial nature of the phenomena is pointed out, and further research will be needed to clarify whether the origin of the inverted hysteresis arises from the same or, on the contrary, from different effects depending on the nature of the contact.

Consequently, we can conclude that the decrease of the hysteresis observed when fullerene derivative SAMs are employed is due to a decrease of the capacitive hysteresis observed for PSCs with TiO_2 as ESC.[14] Moreover, for samples where fullerene SAM is observed, the noncapacitive hysteresis of the $J-V$ curve under dark is also observed for low scan rates in inverted PSCs with organic selective contacts and in devices with TiO_2 as ESC.[14] To this extent, PSCs with fullerene derivative SAM are located half way between both types of PSCs, as present lower capacitive hysteresis than samples with TiO_2 contact and higher capacitive hysteresis than inverted cells with organic contacts where capacitive hysteresis is practically negligible.

Moreover, the variation of the bridging group between the fullerene and the benzoic acid, fullerenes **2** and **3**, does not introduce any significant change on the performance of the PSCs (see Figure 2). Compounds **2** and **3** present the same bandgap (see Table S1) and LUMO position (see Table S2) and induce a PL quenching of the perovskite quite similar, thus indicating that comparable charge injecting properties are induced; therefore the effect of the connecting cyclohexane and pyrrolidine groups induces a negligible effect on the final cell performance. However, the properties induced by the fullerene derivative **1** are significantly changed from the reference fullerene **3** when the connecting part containing the carboxylic group is kept unchanged but a couple of cyanide groups are introduced into the fullerene framework (see Figure 1a). Cyanides are electron withdrawing groups that cause a higher polarization of the molecule. Cyanide groups do not significantly change the bandgap compared to the **3** derivative (see Table S1), but they have a strong effect on the LUMO energy position, which decreases in 20−14 meV compared to the **2**/**3** counterparts, respectively (see Table 1).

A new set of samples has been prepared using a **1** SAM (see Table 1 and Figure 4a). Again, the use of a SAM reduces the $J-V$ curve hysteresis, but with derivative **1**, the efficiency of the PSC increases mainly due to the increase of the measured photocurrent. Note that, for scan rates on the order of the one used in this work (50 mV/s), the stabilized photocurrent lies between forward and reverse curves.[27] The origin of this beneficial effect could be ascribed to the direct contact between the highly polar cyanide groups and the perovskite layer, thus allowing an enhanced coupling of the fullerene−perovskite interface. However, an effect of SAM that changes the wettability of the substrate affecting the morphology of the perovskite layer[28] needs a detailed study beyond the scope of this manuscript. In addition, a strong PL quenching of the perovskite emission has also been observed when the **1** SAM is used (see Figure S5). Note that when the compact layer is removed a partial PL quenching it is also observed (see Figure S5). This fact can be attributed to an increase of surface recombination as the increase of dark current points out (see Figure S4). However, the PL quenching when SAM is added is stronger, thus indicating a significant enhancement of the charge carrier injection. An improved design of the anchoring groups of the fullerene derivatives, as well as the coupling enhancement of the fullerene−perovskite interface induced by the introduction of compatible functional groups, e.g., cyanide groups, provide a broad range of possibilities for the exploration of the PSCs performance by means a simple approach consisting in the insertion of an interfacial SAM layer.

Finally, we have studied the effect of removing the compact TiO_2 ESC, but maintaining the TiO_2 scaffold. When the ESC is removed, the efficiency of the device is severely affected (see Table 1 and Figure 4b), mainly due to the strong decrease of photocurrent, indicating the important role of the compact layer. A detailed analysis of the scaffold effect is beyond the scope of this work. We have already reported that ESC plays a fundamental role in the control of interfacial recombination.[29] Nevertheless, when **1** SAM is employed, there is practically no current decrease (see Figure 4c) due to the interfacial passivation effect induced by the SAM. The use of SAM reduced the hysteresis even when no ESC is present (see Figure 4d and HI in Table 1). However, in the case of NCL samples, the reduction of hysteresis induced by the presence of SAM is significantly lower (see Figure 4d) than in the case of samples with ESC. Several reasons could affect the efficiency of SAM for hysteresis mitigation when no ESC is present: the reactivity of the surface is different, the monolayer quality on FTO may not be as good as on TiO_2, or probably the charge transfer between fullerene and FTO or TiO_2 could differ significantly. Further analysis is needed to clarify this important question that relates contact nature and hysteresis effect. The use of an appropriated fullerene derivative as **1** can significantly mitigate the impact of removing the CL on the J_{sc}; further mitigation of the hysteresis effect by exploring suitable modifications of the fullerene derivative could allow the complete removal of the inorganic ESC, which could provide high impact benefits from the industrial point of view, as it will permit a simplification of the device configuration and processing; for instance, it would avoid a high temperature step in the preparation of PSCs.

In summary, we have analyzed PSCs with different [60]fullerene derivative SAMs at the ESC−perovskite interface, which induces in all the cases an important reduction of the $J-V$ curve hysteresis. We have determined that the hysteresis reduction is due to the decrease of the capacitive hysteresis typically observed for oxide-based anodes in PSCs. SAM samples also present noncapacitive hysteresis in the dark $J-V$ curve, observed at low scan rates, typically observed in inverted PSCs with organic contacts and, to a lesser extent, in standard PSCs with compact TiO_2 ESC. To this extent, PSCs with SAMs of fullerene derivatives are midway devices between standard and inverted PSCs. In addition, we have determined that the design of new fullerene derivatives plays a very important role in the overall solar cell performance, as it has been demonstrated by the inclusion of cyanide groups that enhance the direct coupling with the perovskite layer, thus improving the solar cell parameters, as photocurrent, compared to the reference device with no SAM. However, other aspects as the increase of recombination need to be controlled to optimize the system. The beneficial effect of the SAM can even be extended to the complete removal of the ESC. We have observed that only a slight reduction of the hysteresis is observed when **1** SAM is used with no compact TiO_2 layer; the **1** SAM passivates the FTO surface, thus maintaining the device photocurrent. This work explains the origin of the hysteresis reduction when a fullerene derivative SAM is employed and paves the way for a

DOI: 10.1021/acs.jpclett.6b02103
J. Phys. Chem. Lett. XXXX, XXX, XXX−XXX

future enhancement of PSCs by means of a tailored design of the fullerene molecules that could actuate as an ESC by themselves, without further need of a TiO_2 compact layer.

METHODS

Chemicals. Titanium diisopropoxidebis(acetylacetonate), lead chloride ($PbCl_2$), dimethylformamide (DMF), anhydrous chlorobenzene, lithium bis(trifluoromethylsulfonyl)imide (Li-TFSI), and 4-*tert*-butylpiridine (TBP) were purchased from Sigma-Aldrich. TiO_2 18NRT paste was purchased from Dyesol, and methylammonium iodide (MAI) was purchased from TCI. All the materials were used as received. The different fullerene derivatives were synthesized at IMDEA Institute as detailed below.

Synthesis of [60]Fullerenes Derivatives. **[60]Fullerene 3**: A mixture of 4-carboxybenzaldehyde (104 mg, 0.70 mmol), C_{60} (100 mg, 0.14 mmol) and sarcosine (25 mg, 0.28 mmol) were dissolved in toluene, and the mixture was refluxed for 5 h. The reaction mixture was allowed to reach room temperature and the solvent was removed under vacuum. The crude was purified by flash column chromatography on SiO_2, using CS_2/toluene and then toluene/ethyl acetate (2:1). The black solid obtained was further purified by repeated (3x) precipitation and centrifugation in methanol to yield the corresponding hybrids as black solids. ^{1}H NMR (DMSO-d_6, 300 MHz, 298 K) δ 13.0 (s, 1H), 8.04 (d, J = 7.6 Hz, 2H), 7.94 (d, J = 7.8 Hz, 2H), 5.22 (s, 1H), 5.11 (d, J = 9.4, 1H), 4.35 (d, J = 9.4 Hz, 1H), 3.17 (s, 3H).

[60]Fullerene 2: In a dried 500 mL round-bottom flask, 358 mg (0.497 mmol) of C_{60} was dissolved in 250 mL of dry toluene and sonicated for 15 min. 3,4-Bis(bromomethyl)-benzoic acid (156.2 mg 0.507 mmol), potassium iodide (585 mg 3.5 mmol), and 18-Crown-6 (250 mg 0.94 mmol) were sequentially added while stirring under dry nitrogen. The reaction mixture was stirred and heated at reflux for 14 h. The reaction mixture was allowed to reach room temperature, and the solvent was removed under vacuum. The crude was purified by flash column chromatography on SiO_2 using (CS_2/toluene and then toluene/THF (2:1)). The black solid obtained was further purified by repeated (3x) precipitation and centrifugation in methanol to yield the corresponding hybrid as black solid. ^{1}H NMR (DMSO-d_6, 300 MHz, 298 K) δ 13.1 (s, 1H), 8.35 (d, J = 1.6 Hz, 1H), 8.14 (dd, J = 7.8 Hz, J = 1.6 Hz, 1H), 7.90 (d, J = 7.8 Hz, 1H), 5.06 (m, 2H), 4.66 (m, 2H).

[60]Fullerene 1: A mixture of 4-carboxybenzaldehyde (14.2 mg, 0.09 mmol), C_{60}-CN_2 (80 mg, 0.10 mmol), and sarcosine (41.4 mg, 0.47 mmol) was dissolved in chlorobenzene (20 mL), and the mixture was refluxed for 20 h. The reaction mixture was allowed to reach room temperature and the solvent was removed under vacuum. The crude was purified by flash column chromatography on SiO_2, using CS_2/toluene and then toluene/THF (2:1). The black solids obtained was further purified by repeated (3x) precipitation and centrifugation in methanol to yield the corresponding hybrids as black solids. ^{1}H NMR (DMSO-d6, 300 MHz, 298 K) δ 13.0 (s, 1H), 8.25−7.59 (m), 5.02−4.56 (m), 2.90−2.60 (m). MS-ESI m/z 950.1 $[M + H]^+$.

Solar Cell Fabrication. Fluorine doped tin oxide (FTO) coated glass substrates (Pilkington TEC15, ∼ 15Ω/sq) were etched with zinc powder and HCl (2M). The substrates were sonicated for 15 min in a solution of Milli-Q water and soap (Hellmanex), rinsed with Milli-Q water, sonicated for 15 min in a solution of ethanol, rinsed with acetone and dried with compressed air. After that, a UV/ozone treatment was performed for 15 min. TiO_2 compact layer was deposited onto the substrates by spray pyrolysis at 450 °C, using titanium diisopropoxidebis(acetylacetonate) in ethanol (1:39, v/v), with oxygen as carrier gas. Mesoporous TiO_2 layer was deposited by spin coating at 6000 rpm during 40 s using TiO_2 paste diluted in ethanol (1:3.5, weight ratio). After drying at 80 °C 10 min, it was heated at 470 °C for 30 min and cooled down to room temperature. The different fullerene derivatives were dissolved in chlorobenzene (2 mg/mL) and filtered with a 0.2 μm PTFE filter. The substrates were heated 10 min at 120 °C, immersed in these solutions for 24 h, rinsed with chlorobenzene, and then dried for 10 min at 120 °C. The perovskite solution was prepared by mixing 2.64 M of methylammonium iodide and 0.88 M of lead chloride at a 3:1 mol ratio in DMF. The substrates were heated 10 min at 60 °C, and then the solution was spin-coated at 500 rpm for 5s and 2000 rpm for 60 s in air conditions. After the deposition, the substrates were heated at 100 °C during 90 min in an oven under air stream. Spiro-OMeTAD was deposited by spin coating at 4000 rpm for 30 s. The spiro-OMeTAD solution was prepared by dissolving 72.3 mg of spiro-OMeTAD, 28.8 μL of TBP, and 17.5 μL of a stock solution of 520 mg/mL of Li-TFSI in acetonitrile, in chlorobenzene. The deposition of 60 nm of gold was carried out by thermal evaporation at 10^{-6} mbar. Samples were prepared under air conditions, and the humidity can vary in our laboratory between 30 and 60%; consequently, samples prepared with different conditions cannot be straightforwardly compared among them. Our approach is to prepare reference samples for all the batches and compare each sample with its respective reference (see Table 1).

Characterization. The current−voltage curves were measured with a scan rate of 50 mV/s in Abet Technologies Sun 2000 Class A solar simulator with a Keithley 2612 Source Meter, AM1.5G and 100 mW·cm^{-2}. The measurements were performed using a shadow mask whose area was 0.089 cm^2. For the PL measurements, a commercial red laser diode (650 nm) was used as the excitation source. The measurements were carried out using a spectrophotometer CCD based detector (charge-coupled device, AndoriDUS DV 420A-OE) coupled with a spectrograph as a diffraction grating (Newport 77400).

ASSOCIATED CONTENT

Supporting Information

The Supporting Information is available free of charge on the ACS Publications website at DOI: 10.1021/acs.jpclett.6b02103.

Normalized absorbance spectra and cyclic voltammetry measurements of the fullerene derivatives; photoluminescence spectra and dark current of the complete devices (PDF)

AUTHOR INFORMATION

Corresponding Authors

*E-mail: nazmar@ucm.es.

*E-mail: sero@uji.es.

Notes

The authors declare no competing financial interest.

ACKNOWLEDGMENTS

This work was supported by the European Research Council (ERC-320441-Chir*all*carbon), the CAM (FOTOCARBON Project S2013/MIT-2841), MINECO of Spain (Projects

DOI: 10.1021/acs.jpclett.6b02103
J. Phys. Chem. Lett. XXXX, XXX, XXX−XXX

MAT2013-47192-C3-1-R, CTQ2014-52045-R, and MAT2015-70611-ERC) and by Generalitat Valenciana (Project PROMETEOII/2014/020). We acknowledge SCIC from the University Jaume I for help with SEM characterization. B.C.H is grateful to the support of the National Council of Technological and Scientific Development (CNPq), Brazil, through the Science without Borders program.

REFERENCES

(1) Kim, H.-S.; Lee, C.-R.; Im, J.-H.; Lee, K.-B.; Moehl, T.; Marchioro, A.; Moon, S.-J.; Humphry-Baker, R.; Yum, J.-H.; Moser, J. E.; et al. Lead Iodide Perovskite Sensitized All-Solid-State Submicron Thin Film Mesoscopic Solar Cell with Efficiency Exceeding 9%. *Sci. Rep.* **2012**, *2*, 591.

(2) Lee, M. M.; Teuscher, J.; Miyasaka, T.; Murakami, T. N.; Snaith, H. J. Efficient Hybrid Solar Cells Based on Meso-Superstructured Organometal Halide Perovskites. *Science* **2012**, *338*, 643−647.

(3) Yang, W. S.; Noh, J. H.; Jeon, N. J.; Kim, Y. C.; Ryu, S.; Seo, J.; Seok, S. I. High-Performance Photovoltaic Perovskite Layers Fabricated through Intramolecular Exchange. *Science* **2015**, *348*, 1234−1237.

(4) Jeon, N. J.; Noh, J. H.; Yang, W. S.; Kim, Y. C.; Ryu, S.; Seo, J.; Seok, S. I. Compositional Engineering of Perovskite Materials for High-Performance Solar Cells. *Nature* **2015**, *517*, 476−480.

(5) Jeon, N. J.; Noh, J. H.; Kim, Y. C.; Yang, W. S.; Ryu, S.; Seok, S. I. Solvent Engineering for High-Performance Inorganic−Organic Hybrid Perovskite Solar Cells. *Nat. Mater.* **2014**, *13*, 897−903.

(6) Saliba, M.; Matsui, T.; Seo, J.-Y.; Domanski, K.; Correa-Baena, J.-P.; Nazeeruddin, M. K.; Zakeeruddin, S. M.; Tress, W.; Abate, A.; Hagfeldt, A.; et al. Cesium-Containing Triple Cation Perovskite Solar Cells: Improved Stability, Reproducibility and High Efficiency. *Energy Environ. Sci.* **2016**, *9*, 1989−1997.

(7) Molina-Ontoria, A.; Zimmermann, I.; Garcia-Benito, I.; Gratia, P.; Roldán-Carmona, C.; Aghazada, S.; Graetzel, M.; Nazeeruddin, M. K.; Martín, N. Benzotrithiophene-Based Hole-Transporting Materials for 18.2% Perovskite Solar Cells. *Angew. Chem., Int. Ed.* **2016**, *55*, 6270−6274.

(8) Green, M. A.; Emery, K.; Hishikawa, Y.; Warta, W.; Dunlop, E. D. Solar Cell Efficiency Tables (version 48). *Prog. Photovoltaics* **2016**, *24*, 905−913.

(9) Kazim, S.; Nazeeruddin, M. K.; Grätzel, M.; Ahmad, S. Perovskite as Light Harvester: A Game Changer in Photovoltaics. *Angew. Chem., Int. Ed.* **2014**, *53*, 2812−2824.

(10) Chen, B.; Yang, M.; Priya, S.; Zhu, K. Origin of J−V Hysteresis in Perovskite Solar Cells. *J. Phys. Chem. Lett.* **2016**, *7*, 905917.

(11) Levine, I.; Nayak, P. K.; Wang, J. T.-W.; Sakai, N.; van Reenen, S.; Brenner, T. M.; Mukhopadhyay, S.; Snaith, H. J.; Hodes, G.; Cahen, D. Interface-Dependent Ion Migration/Accumulation Controls Hysteresis in MAPbI3 Solar Cells. *J. Phys. Chem. C* **2016**, *120*, 16399−16411.

(12) Bryant, D.; Wheeler, S.; O'Regan, B. C.; Watson, T.; Barnes, P. R. F.; Worsley, D.; Durrant, J. Observable Hysteresis at Low Temperature in "Hysteresis Free" Organic−Inorganic Lead Halide Perovskite Solar Cells. *J. Phys. Chem. Lett.* **2015**, *6*, 3190−3194.

(13) Tress, W.; Marinova, N.; Moehl, T.; Zakeeruddin, S. M.; Nazeeruddin, M. K.; Gratzel, M. Understanding the Rate-Dependent J-V Hysteresis, Slow Time Component, and Aging in $CH_3NH_3PbI_3$ Perovskite Solar Cells: The Role of a Compensated Electric Field. *Energy Environ. Sci.* **2015**, *8*, 995−1004.

(14) Almora, O.; Aranda, C.; Zarazua, I.; Guerrero, A.; Garcia-Belmonte, G. Noncapacitive Hysteresis in Perovskite Solar Cells at Room Temperature. *ACS Energy Lett.* **2016**, *1*, 209−215.

(15) Bisquert, J.; Cahen, D.; Hodes, G.; Rühle, S.; Zaban, A. Physical Chemical Principles of Photovoltaic Conversion with Nanoparticulate, Mesoporous Dye-Sensitized Solar Cells. *J. Phys. Chem. B* **2004**, *108*, 8106−8118.

(16) Völker, S. F.; Collavini, S.; Delgado, J. L. Organic Charge Carriers for Perovskite Solar Cells. *ChemSusChem* **2015**, *8*, 3012−3028.

(17) Stranks, S. D.; Eperon, G. E.; Grancini, G.; Menelaou, C.; Alcocer, M. J. P.; Leijtens, T.; Herz, L. M.; Petrozza, A.; Snaith, H. Electron-Hole Diffusion Lengths Exceeding 1 Micrometer in an Organometal Trihalide Perovskite Absorber. J. *Science* **2013**, *342*, 341−344.

(18) Xing, G.; Mathews, N.; Sun, S.; Lim, S. S.; Lam, Y. M.; Grätzel, M.; Mhaisalkar, S.; Sum, T. C. Long-Range Balanced Electron- and Hole-Transport Lengths in Organic-Inorganic $CH_3NH_3PbI_3$. *Science* **2013**, *342*, 344−347.

(19) Tao, C.; Neutzner, S.; Colella, L.; Marras, S.; Srimath Kandada, A. R.; Gandini, M.; Bastiani, M. D.; Pace, G.; Manna, L.; Caironi, M.; et al. 17.6% Stabilized Efficiency in Low-Temperature Processed Planar Perovskite Solar Cells. *Energy Environ. Sci.* **2015**, *8*, 2365−2370.

(20) Li, Y.; Zhao, Y.; Chen, Q.; Yang, Y.; Liu, Y.; Hong, Z.; Liu, Z.; Hsieh, Y.-T.; Meng, L.; Li, Y.; et al. Multifunctional Fullerene Derivative for Interface Engineering in Perovskite Solar Cells. *J. Am. Chem. Soc.* **2015**, *137*, 15540−15547.

(21) Wojciechowski, K.; Stranks, S. D.; Abate, A.; Sadoughi, G.; Sadhanala, A.; Kopidakis, N.; Rumbles, G.; Li, C.-Z.; Friend, R. H.; Jen, A. K. Y.; et al. Heterojunction Modification for Highly Efficient Organic−Inorganic Perovskite Solar Cells. *ACS Nano* **2014**, *8*, 12701−12709.

(22) Sanchez, R. S.; Gonzalez-Pedro, V.; Lee, J.-W.; Park, N.-G.; Kang, Y. S.; Mora-Sero, I.; Bisquert, J. Slow Dynamic Processes in Lead Halide Perovskite Solar Cells. Characteristic Times and Hysteresis. *J. Phys. Chem. Lett.* **2014**, *5*, 2357−2363.

(23) Almora, O.; Zarazua, I.; Mas-Marza, E.; Mora-Sero, I.; Bisquert, J.; Garcia-Belmonte, G. Capacitive Dark Currents, Hysteresis, and Electrode Polarization in Lead Halide Perovskite Solar Cells. *J. Phys. Chem. Lett.* **2015**, *6*, 1645−1652.

(24) Carrillo, J.; Guerrero, A.; Rahimnejad, S.; Almora, O.; Zarazua, I.; Mas-Marza, E.; Bisquert, J.; Garcia-Belmonte, G. Ionic Reactivity at Contacts and Aging of Methylammonium Lead Triiodide Perovskite Solar Cells. *Adv. Energy Mater.* **2016**, *6*, 1502246.

(25) Stumpp, M.; Ruess, R.; Horn, J.; Tinz, J.; Richter, C.; Schlettwein, D. I−V Hysteresis of Methylammonium Lead Halide Perovskite Films on Microstructured Electrode Arrays: Dependence on Preparation Route and Voltage Scale. *Phys. Status Solidi A* **2016**, *213*, 38−45.

(26) Tress, W.; Correa Baena, J. P.; Saliba, M.; Abate, A.; Graetzel, M. Inverted Current−Voltage Hysteresis in Mixed Perovskite Solar Cells: Polarization, Energy Barriers, and Defect Recombination. *Adv. Energy Mater.* **2016**, *6*, 1600396.

(27) Christians, J. A.; Manser, J. S.; Kamat, P. V. Best Practices in Perovskite Solar Cell Efficiency Measurements. Avoiding the Error of Making Bad Cells Look Good. *J. Phys. Chem. Lett.* **2015**, *6*, 852−857.

(28) Bi, C.; Wang, Q.; Shao, Y.; Yuan, Y.; Xiao, Z.; Huang, J. Non-wetting surface-driven high-aspect-ratio crystalline grain growth for efficient hybrid perovskite solar cells. *Nat. Commun.* **2015**, *6*, 7747.

(29) Juarez-Perez, E. J.; Wuβler, M.; Fabregat-Santiago, F.; Lakus-Wollny, K.; Mankel, E.; Mayer, T.; Jaegermann, W.; Mora-Sero, I. Role of the Selective Contacts in the Performance of Lead Halide Perovskite Solar Cells. *J. Phys. Chem. Lett.* **2014**, *5*, 680−685.

DOI: 10.1021/acs.jpclett.6b02103
J. Phys. Chem. Lett. XXXX, XXX, XXX−XXX